https://doi.org/10.5194/egusphere-2026-4
Preprint. Discussion started: 2 February 2026

Physical Interpretation and Implications of Convective Impulses in Thunderstorms Based on Lightning and Polarimetric Radar Observations

Chuanhong Zhao,[1,2]* Yijun Zhang,[2,3]* Dong Zheng,[4] Liangtao Xu,[4] Wen Yao,[4]

Affiliations

[1]Climate Change and Resource Utilization in Complex Terrain Regions Key Laboratory of Sichuan Province, School of Atmospheric Sciences, Chengdu University of Information Technology, Chengdu, 610225, China.

[2]Department of Atmospheric and Oceanic Sciences & Institute of Atmospheric Sciences, Fudan University, Shanghai, 200438, China.

[3]Shanghai Key Laboratory of Ocean-land-atmosphere Boundary Dynamics and Climate Change & Shanghai Frontiers Science Center of Atmosphere-Ocean Interaction, Fudan University, Shanghai, 200438, China.

[4]State Key Laboratory of Severe Weather Meteorological Science and Technology & CMA Key Laboratory of Lightning, Chinese Academy of Meteorological Sciences, Beijing 100081, China.

Corresponding authors: Dr. Yijun Zhang & Dr. Chuanhong Zhao are the co-corresponding authors.

E-mail: zhangyijun@fudan.edu.cn; zch@cuit.edu.cn

https://doi.org/10.5194/egusphere-2026-4
Preprint. Discussion started: 2 February 2026

Abstract

Convective impulses (CIs) occur in thunderstorms and are strongly associated with severe convection, often contributing to hazardous weather events. However, the underlying physical mechanisms governing CIs remain poorly understood. In this study, multiple CI events were identified in two selective isolated thunderstorms and analyzed from the perspective of the cloud life cycle using polarimetric radar and lightning observations. We investigated the roles of environmental conditions and cloud microphysics in CI events. Our results indicate a pronounced increase in supercooled liquid water and graupel content prior to CI occurrence. The breakup of raindrops is closely linked to the observed increase in supercooled raindrops, suggesting that the fragmentation of large raindrops below the melting layer contributes to raindrop multiplication at subfreezing temperatures. These smaller raindrops subsequently freeze into graupel-like particles, releasing latent heat that may enhance convection and/or lightning activity. This hypothesized physical mechanism is further supported by idealized numerical simulations, which demonstrate that the updraft intensity varies with the efficiency of raindrop breakup. Additionally, large raindrops involved in the breakup process originate from the coalescence of raindrops during the initial pre-CI event, whereas graupel melting or shedding plays a role in subsequent pre-CI events. This improves the understanding of CIs following precipitation loading, melting, and evaporation within a near-stationary thunderstorm cell. These findings reveal a likely physical mechanism contributing to CI events and offer new insights into thunderstorm microphysics and dynamics.

Short summary

In contrast to the relatively steady and vigorous convection observed in organized thunderstorms, convective impulses (CIs) within less organized, single-cell storms are inherently more challenging to predict. Here, a conceptual hypothesis is proposed to elucidate the physical mechanisms governing CI formation, supported by polarimetric radar and lightning observations and idealized numerical simulations. The results improve our knowledge of thunderstorm dynamics and microphysics.

Keywords: thunderstorm; lightning; cloud microphysics; polarimetric radar

1.Introduction

Thunderstorms, which are intense convective clouds, play important roles in weather and

https://doi.org/10.5194/egusphere-2026-4
Preprint. Discussion started: 2 February 2026

climate; produce copious amounts of precipitation, lightning, and tornadoes; and affect cloud radiative forcing (MacGorman and Rust, 1998; Williams et al., 2005; Zhang et al., 2009). Explaining how the convective impulse (CI, which is often associated with the convective updraft speed, lightning flash rate, and radar reflectivity) occurs in thunderstorms is always challenging but is key for understanding and simulating thunderstorms (Zipser et al., 2006; Markowski and Richardson, 2010; Bruning et al., 2024; Zhao et al., 2025).

Unsteady updrafts tied to thermal bubbles generally indicate CI events (Bruning et al., 2024). Three-dimensional thunderstorm modeling studies have clarified thunderstorm development by placing a warm bubble into low levels of a conditionally unstable environment (Markowski and Richardson, 2010). Warm bubbles initiate a sustained updraft, and the subsequent evolution is dependent on the vertical wind shear and the convective available potential energy (CAPE) of the environment (Markowski and Richardson, 2010; Grabowski and Morrison, 2021). Observational studies of the spatial distribution of severe storms have indicated that intense convection strongly preferentially occurs over land and that the frequency of lightning is higher than that over the ocean (Orville and Henderson, 1986; Zipser et al., 2006; Cecil et al., 2014). The thermodynamic difference between land and ocean may account for this difference (Williams and Stanfill, 2002; Thornton et al., 2017; Grabowski and Morrison, 2021; Grabowski, 2023; Qie et al., 2024), although some studies note that aerosol concentrations may also be a factor (Rosenfeld and Lensky, 1998; Koren et al., 2004; Rosenfeld et al., 2008; Fan J. et al., 2018; 2025). Specifically, substantial storm-scale variability in dominant thermodynamic controls on the strength of convective updrafts coupled with substantial updraft and aerosol variability in many given events are poorly quantified by observations and present further challenges for isolating aerosol effects (Varble et al., 2023).

Previous studies have investigated environmental features corresponding to severe storms, and the results have indicated that thunderstorm intensity is closely related to strong CAPE and wind shear (Brooks et al., 2003; Liu N. et al., 2020). CAPE is a necessary, albeit insufficient, condition for convection initiation; typical thunderstorms occur in environments with CAPE values higher than 1000 J kg^{-1} (Lucas et al., 1994; Markowski and Richardson, 2010). Wind shear is the principal factor controlling the organization of convective storms (e.g., single-cell vs. multicell vs. supercell storms) (Markowski and Richardson, 2010). Although severe weather tends to be more widespread

https://doi.org/10.5194/egusphere-2026-4
Preprint. Discussion started: 2 February 2026

when high shear accompanies significant CAPE, less organized, single-cell storms with briefly intense updrafts can also produce severe weather (of the pulse variety) in high-CAPE, weak-shear environments (Markowski and Richardson, 2010).

The knowledge above essentially clarifies convection development in the real world, as CAPE, wind shear, and/or aerosol concentrations are unlikely to briefly change to dominate these relatively short-lived CI events in isolated thunderstorms. However, CI events in isolated thunderstorms objectively exist; thus, convective cloud development or behavior characteristics during subsequent evolution are unclear, which explains why the CAPE and wind shear cannot be perfect proxies for thunderstorms (Liu N. et al., 2020). The impulses of convective strength in the subsequent evolution of thunderstorms are strongly modulated by cloud microphysical processes, which are generally accepted by cloud physicists, although some mechanisms that are theorized to drive convective invigoration with increased aerosol loading are controversial (Koren et al., 2004; Rosenfeld et al., 2008; Thornton et al., 2017; Fan J. et al., 2018; Dagan et al., 2020; Grabowski and Morrison, 2020, 2021; Liu N. et al., 2020; Varble et al., 2023). According to Fan et al. (2025), condensational invigoration is most significant under clean atmospheric conditions when many ultrafine particles are introduced, and freezing-induced invigoration can be significant under similarly clean conditions when many relatively large-sized particles are added, as supported by both modeling and observational evidence.

Nevertheless, while the above knowledge can clarify the convective enhancement of thunderstorms that are moving and organized (i.e., the CAPE or aerosol concentration may increase with the variety of environments), it is ineffective for understanding the short-term impulses of convective intensity (i.e., multiple CI events) in isolated thunderstorms or near-stationary thunderstorm cells. Here, the objective of this study is to explore the microphysics and kinematics and the underlying mechanism that are attributed to CI events on the basis of observations of the evolutionary cycle of isolated thunderstorms and numerical simulations.

2.Data and methods

We select two special isolated thunderstorm cells during the warm season over southern China on the basis of observations from a lightning location system, dual-polarization radar, and ERA-Interim reanalysis data. One thunderstorm was a near-stationary thunderstorm with high CAPE,

https://doi.org/10.5194/egusphere-2026-4
Preprint. Discussion started: 2 February 2026

weak wind shear, and a clean environment; this thunderstorm is referred to as case A and occurred on 20 June 2016. The other thunderstorm was a moving thunderstorm with significant CAPE, strong wind shear, and a clean environment; this thunderstorm is referred to as case B and occurred on 13 June 2016. In this study, the evolutionary cycle of thunderstorms is defined as the duration from the first radar echo (i.e., the radar volume scan in cases where the horizontal reflectivity (Z_H) is ≥ 5 dBZ when clouds are first detected by radar) to cloud collapse. The evolutionary cycles of the two thunderstorms are displayed in Fig. S1 and S2. To ensure the quality of the radar and lightning data, the locations of the centers of the two thunderstorms meet the conditions and are restricted to approximately the analyzed areas, which are the regions of overlapping coverage between the radar radii of 25−100 km and the lightning-location-system network center radius of 70 km.

2.1. Lightning location system

A low-frequency E-field detection array (LFEDA, 10 sensors, as marked by orange dots in Fig. S3) with the ability to describe three-dimensional structures of intracloud lightning and/or cloud-to-ground lightning was utilized to identify lightning events in this analyzed area. The detection efficiency and mean location error of the LFEDA for triggered lightning were approximately 100% and 102 m, respectively (Shi et al., 2017; Fan X. et al., 2018), which is the highest efficiency of lightning location systems in Guangzhou, China (Chen et al., 2012). The LFEDA, operates in the low-frequency range (160 Hz~600 kHz) and locates discharge pulse events (DPEs) via the time-of-arrival method. The quality control method for the DPEs followed that of Liu Z. et al. (2020). The method for grouping DPEs into flashes followed those of Shi et al. (2017) and Zheng et al. (2019); that is, a potential flash DPE must have occurred within 400 ms of the previous DPE and within 4 km and 600 ms of any other flash DPE.

2.2. Radar observations and preprocessing

The radar data were provided by the Guangzhou S-band dual-polarization radar (GZ radar, as marked by the white triangle in Fig. S3). The configurations of this radar are as follows: a range resolution of 250 m, a beam width of 1°, and an azimuth resolution of 1°. This radar works in the mode of volume coverage pattern 21, which consists of nine plan position indicator scans with a volumetric update time of 6 minutes. A quality control procedure was carried out to remove ground clutter, anomalous propagation, and biological scatter (Zhao et al., 2021a, b, 2022, 2024a). The

https://doi.org/10.5194/egusphere-2026-4
Preprint. Discussion started: 2 February 2026

differential reflectivity (Z_{DR}) was calibrated during light rainfall periods, and the calibration accuracy ranged from 0.1–0.2 dB (Bringi and Chandrasekar, 2001). The quality-controlled radar data were interpolated onto a Cartesian grid at a horizontal resolution of 250 m and a vertical resolution of 500 m from 0.5 to 20 km above the mean sea level via nearest neighbor and vertical linear interpolation (Zhao et al., 2024a, b).

2.3. Environmental observations and ERA-Interim data

The environmental temperature information was provided by sounding data obtained from the Qingyuan meteorological observatory (as marked by blue diamonds in Fig. S3). The hourly observed particulate matter ($PM_{2.5}$) mass concentration data were provided by the Ministry of Ecology and Environment of the People's Republic of China (Wang and Zhang, 2020), and three ground sites for aerosol concentrations within the analyzed area were used, as marked by blue dots in Fig. S3. Six-hourly ERA-Interim reanalysis data, with a 0.175°×0.175° horizontal resolution, were utilized (Dee et al., 2011).

2.4. Analytical method

Lightning activity and echo-top height provide kinematic variation in the evolutionary cycle of isolated thunderstorms with temporal resolution considerations (Zipser et al., 2006; Carey and Rutledge, 2000). Benefiting from polarimetric radar observations, warm- and mixed-phase microphysics, even the "fingerprint" of microphysical processes, were derived to study how microphysical processes increase convective strength (Carey and Rutledge, 2000; Kumjian and Prat, 2014; Hu and Ryzhkov, 2022; Kumjian et al., 2022; Zhao et al., 2025).

Specifically, the ice and rain water contents were estimated from the GZ radar measurements via the difference reflectivity (Z_{DP}) method (Golestani et al., 1989; Carey and Rutledge, 2000). The precipitation-sized ice particles were likely more spherically symmetrical or tumble, resulting in a near-zero Z_{DR} (Pruppacher and Klett, 1997). Therefore, ice particles can be regarded as "effective spheres", and the Z_{DP} is solely influenced by raindrops. The horizontal reflectivity of raindrops can be derived from the relationship between horizontal reflectivity and Z_{DP} (raindrops), where the empirical relationship was derived from 2-year disdrometer data in Guangdong Province (Li et al., 2020), and the residual difference in the observed horizontal reflectivity is associated with ice particles. On the basis of the scattering properties of typical graupel (Zhao et al., 2021b), if $Z_H \geq 35$

https://doi.org/10.5194/egusphere-2026-4
Preprint. Discussion started: 2 February 2026

dBZ, the corresponding ice mass was regarded as a graupel mass, as used in Carey and Rutledge (2000). The standard error for the relationship between the horizontal reflectivity and Z_{DP} is consistently approximately 1 dB (Carey and Rutledge, 2000). The estimated mass is proportional to the actual mass and depends on the variability in the intercept parameter of an assumed inverse exponential distribution for the hydrometeor and its density; thus, the trends of the estimated mass are deemed sufficient for application in this study.

Once the ice water content was determined, the total number concentration (N_t) of ice particles larger than 0.1 mm was computed; the relationship follows that of Hu and Ryzhkov (2022). Notably, the radar retrieval techniques were valid mainly in the stratiform parts of storm systems where graupel and hail are usually absent, and the derived ice microphysics were representative of storm areas where the radar reflectivity does not exceed 30 dBZ. The quantified method for the polarimetric “fingerprint” of each warm-rain process follows that of Kumjian and Prat (2014). The mass-weighted mean drop diameter (D_m, mm) was retrieved from Z_H and Z_{DR}, following Tokay et al. (2020); the absolute bias of D_m was 0.31-0.36 mm.

3.Results

3.1. Overview of two isolated thunderstorms in the environment and their development

CAPEs derived from the 6-hourly averaged ERA-Interim reanalysis data and the averaged 1-hourly concentration observations of particulate matter ($PM_{2.5}$) from three ground sites prior to the occurrences of these two isolated thunderstorms (case A and case B) show lower CAPE and $PM_{2.5}$ concentrations in case A (1277 J kg^{-1} and 23 μg m^{-3}) and higher CAPE and $PM_{2.5}$ concentrations in case B (1504 J kg^{-1} and 47 μg m^{-3}, respectively). The $PM_{2.5}$ concentrations suggest that the environments prior to the presence of these two isolated thunderstorms were clean, especially for case A. The conditions of relative humidity and wind shear derived from the 6-hourly averaged ERA-Interim reanalysis data indicate more vapor and severe wind shear in case B than in case A (Fig. 1a, b). The environments suggest conditions preferable for thunderstorm development in case B.

https://doi.org/10.5194/egusphere-2026-4
Preprint. Discussion started: 2 February 2026

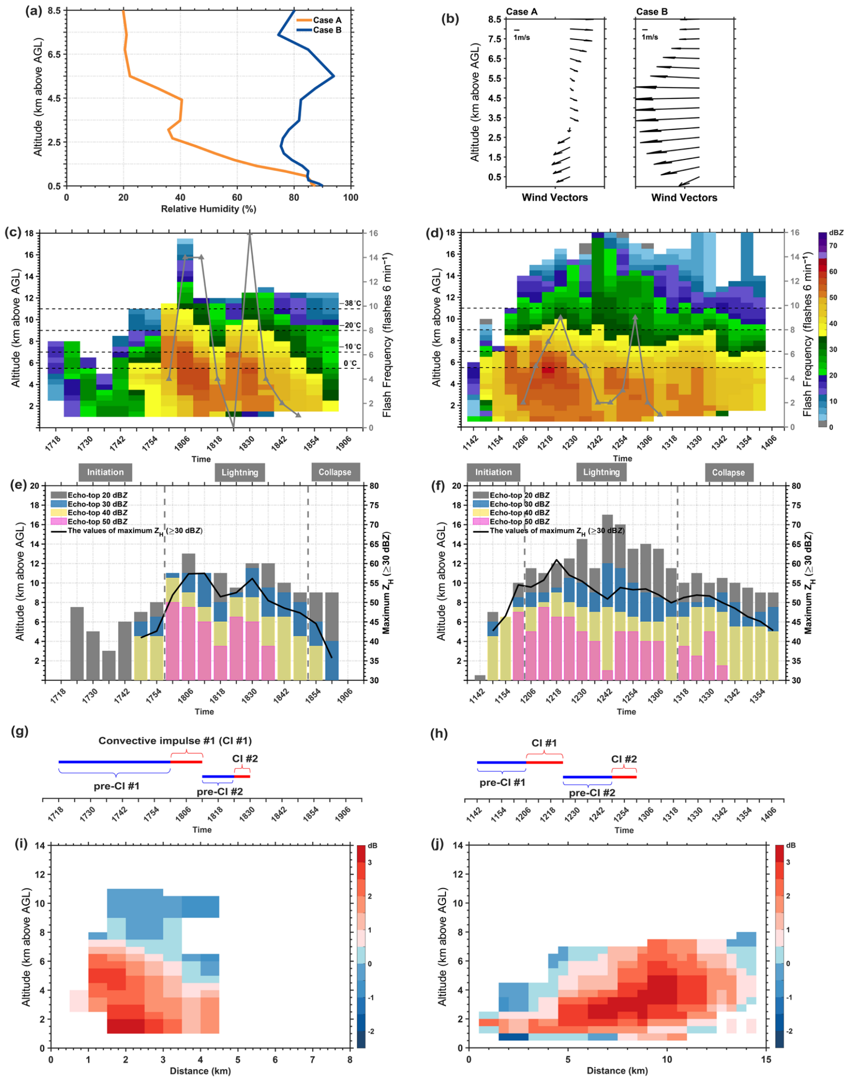

Figure 1. Overview of two isolated thunderstorms in the environment and their development. The conditions of relative humidity and wind shear were derived from 6-hourly averaged ERA-Interim reanalysis data prior to the occurrence of these two isolated thunderstorms (case A occurred on 20 June 2016; case B occurred on 13 June 2016). (**a**) Relative humidity; the orange line indicates case A, and the blue line indicates case B. (**b**) Vertical wind vectors; the left column represents case A, and the right column represents case B. (**c**) and (**d**) show the evolution of the maximum Z_H values for every height layer (a vertical resolution of 500 m over 0.5 to 20 km of a radar volume scan), with cloud development. The left column indicates case A, and the right column indicates case B. The gray lines indicate the flash frequency for a radar volumetric update time of 6 minutes. The black dashed lines indicate the 0°C, −10°C, −20°C, and −38°C isotherm heights. The echo-top heights of 20 dBZ (gray bars), 30 dBZ (blue bars), 40 dBZ (yellow bars), and 50 dBZ (pink bars) in every radar volume scan with cloud development are shown in (**e**) case A and (**f**) case B, respectively. The black lines indicate the evolution of the maximum Z_H values

https://doi.org/10.5194/egusphere-2026-4
Preprint. Discussion started: 2 February 2026

of a radar volume scan (neglecting values < 30 dBZ). In addition, the gray dashed lines divide the evolutionary cycle of thunderstorms into three stages (i.e., initiation, lightning, and collapse). The durations of the convective impulse (CI) and pre-CI are shown; each case involves two CI events, and two pre-CI events are shown in (**g**) case A and (**h**) case B. The overlapping time between the pre-CI and CI indicates CI initiation, and vice versa. Vertical cross-sections of the radar differential reflectivity (Z_{DR}) (**i**) at 17:54 in case A and (**j**) at 12:00 in case B.

The evolutionary cycles of these two thunderstorms are derived from radar and lightning observations. Specifically, the evolution of the maximum Z_H values for every height layer (a vertical resolution of 500 m over 0.5 to 20 km of a radar volume scan) is displayed in Fig. 1c and d; the evolutions of the echo-top height and the maximum Z_H value in a radar volume scan are displayed in Fig. 1e and f; and the lightning frequency in a radar volumetric update time of 6 minutes is displayed in Fig. 1c and d. These two thunderstorms are deep convective clouds (Fig. 1c, d). We divided the evolution cycles of these two thunderstorms into three stages according to the lightning activity and echo intensity: initiation, lightning and collapse. For the initiation stage (Fig. 1e, f), the mean values of the echo-top heights (reflectivity thresholds: 30 dBZ and 40 dBZ) in case B are clearly greater than those in case A; in addition, the average maximum Z_H value in case B (48 dBZ) is greater than that in case A (42 dBZ). An echo-top height of 50 dBZ occurs in case B but is absent in case A. These characteristics indicate that the convective strength is greater in case B during the initiation stage. This confirms the above suggestion provided by environmental characteristics.

While environmental characteristics and radar observations during the initiation stage suggest that the thunderstorm in case B is more intense, the convective intensity during the lightning stage is confusing between cases A and B (the average maximum Z_H values are 53 dBZ and 54 dBZ, respectively; the average echo-top heights of 30 dBZ and 40 dBZ in case A are 0.1~0.2 km greater than those in case B, and the average echo-top height of 50 dBZ in case A is 1 km greater than that in case B). Moreover, the lightning frequency also has a higher peak value in case A than in case B. Finally, in case A, the thunderstorm rapidly collapsed, but in case B, it slowly dissipated. These characteristics indicate that the convective intensity of the thunderstorm rapidly changed.

3.2 Convective impulse events

The convective intensity indicated by the lightning frequency, echo-top height of 50 dBZ, and maximum Z_H value clearly displays short-term impulses (Fig. 1c, d, e, and f). We utilized the variation in the lightning frequency to define the duration times of the convective impulse (CI) and

https://doi.org/10.5194/egusphere-2026-4
Preprint. Discussion started: 2 February 2026

pre-CI. There are two CI events and two corresponding pre-CI events in each thunderstorm (Fig. 1g, h). The overlapping time between the pre-CI and CI indicates CI initiation, and vice versa.

In case A (Fig. 1g), the duration of the first CI event ranged from 18:00 to 18:12 (local time), and that of the second CI event ranged from 18:24 to 18:30; the duration of the first pre-CI event ranged from 17:18 to 18:00, and that of the second pre-CI event ranged from 18:12 to 18:24. In case B (Fig. 1h), the duration of the first CI event ranged from 12:06 to 12:24, and that of the second CI event ranged from 12:48 to 13:00; the duration of the first pre-CI event ranged from 11:42 to 12:06, and that of the second pre-CI event ranged from 12:24 to 12:48. The CI event essentially corresponds to the convective enhancement revealed by the lightning activity, echo-top height and maximum Z_H. Thus, to study how cloud microphysics modulate convective intensity, we focus on cloud microphysics during the corresponding pre-CI event.

3.3. Cloud microphysics in the first pre-CI

Latent heat release can be regarded as the energy source for increasing buoyancy (Rosenfeld et al., 2008; Varble et al., 2023), but some debates still exist (e.g., Grabowski and Morrison, 2020). More specifically, observational studies indicate that the nucleation process from abundant supercooled liquid water to graupel is closely related to lightning (Bringi et al., 1997; Smith et al., 1999; Carey and Rutledge, 2000). Graupel is rimed ice precipitation. The "coalescence–freezing" mechanism is often regarded as the most important pathway to the first graupel/hail formation, the first significant electrification and the first lightning flash in warm-based clouds (Braham, 1986; Beard, 1992; Herzegh and Jameson 1992; Bringi et al., 1997; Smith et al., 1999; Carey and Rutledge, 2000; Stolzenburg et al., 2015; Mattos et al., 2017). This mechanism depends on the development of rain drops in warm rain collision–coalescence processes, followed by lofting of the rain drop in the updraft to areas of subfreezing temperatures (which are frequently observed by polarimetric radar, called Z_{DR} column), followed by drop freezing and finally the formation of graupel or small hail.

The logarithmic total water content in cases A and B during the first pre-CI period are shown in Fig. 2a and b. The logarithmic total ice contents in cases A and B during the first pre-CI period are shown in Fig. 2c and d. When the first CI initiates at 18:00 (case A) or 12:06 (case B), graupel sharply occurs, and the contents of warm-phase rainwater and supercooled rainwater reach peak

https://doi.org/10.5194/egusphere-2026-4
Preprint. Discussion started: 2 February 2026

values. The graupel content in case A ($10^{7.7}$ kg) is clearly greater than that in case B ($10^{6.1}$ kg). However, in case B, more liquid water accumulates in less time (corresponding to more favorable moisture and CAPE). In addition, the amount of supercooled rainwater clearly increases beginning at 17:48 in case A, which is approximately 10^3 times greater than that at 17:42.

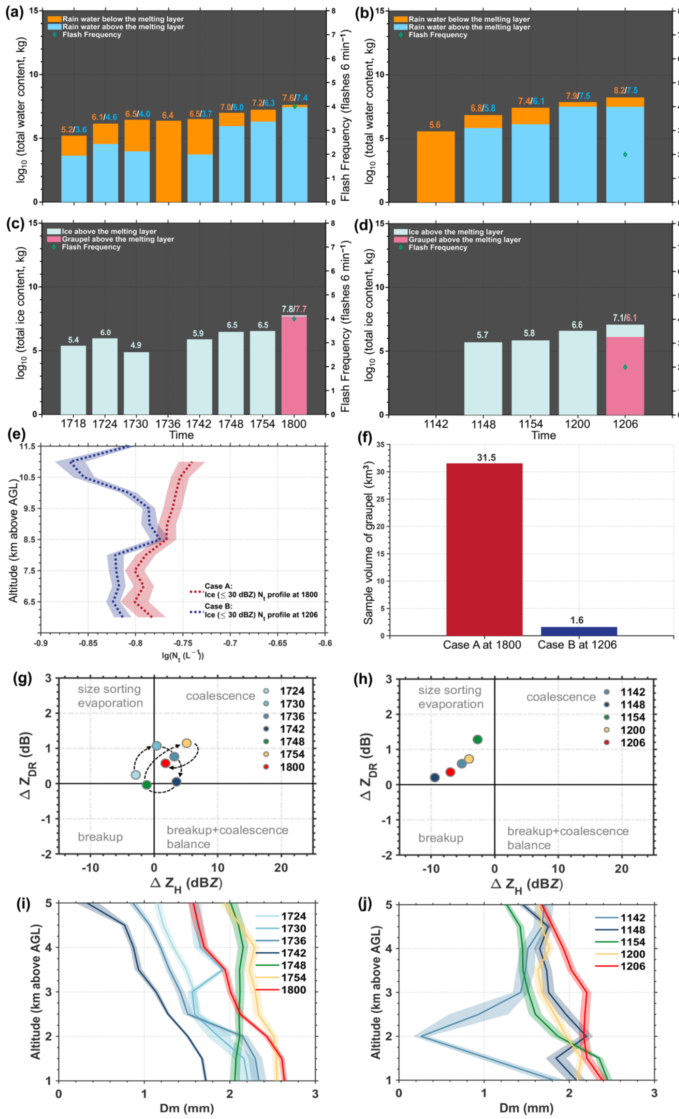

Figure 2. Cloud microphysics in the first pre-CI and comparisons between these thunderstorms. The histogram plots display the logarithmic total water content and the logarithmic total ice content in case A (**a**, **c**) and case B (**b**, **d**). The orange (blue) bars indicate the rainwater content below (above) the melting layer. The cyan and pink bars indicate the contents of ice and graupel above the melting layer, respectively. The numerical values in

https://doi.org/10.5194/egusphere-2026-4
Preprint. Discussion started: 2 February 2026

different colors correspond to the total contents of different hydrometeors (unit, kg). The green diamond indicates the flash frequency. (**e**) The number concentration ($\log_{10}N_t$, L^{-1}) of ice (≤ 30 dBZ) particles when CI initiates. The red and blue dashed lines indicate cases A and B, respectively. (**f**) The radar sample volume of graupel corresponding to the beginning of the CI (unit, km^3). The red histogram indicates case A, and the blue histogram indicates case B. The change in Z_{DR} vs. the change in Z_H over an approximate 3-km rain shaft and the microphysical processes represented by each quadrant or "fingerprint" are annotated: (**g**) case A and (**h**) case B. Each colored dot indicates the changed Z_{DR} and Z_H values over an approximate 3-km rain shaft from one radar volume scan at different times. The retrieved mass-weighted mean drop diameter (D_m) is shown in (**i**) (case A) and (**j**) (case B), the lines indicate the mean values and the shaded area indicates the 95% confidence interval.

a. The microphysical characteristics of ice in the first pre-CI

The latent heat released from supercooled liquid water that freezes and/or rimes into graupel is likely the kinematic source corresponding to the first CI event. From the perspective of the supercooled water content, more abundant supercooled rainwater is present in case B during the last three moments, which seems to suggest that if the number concentrations of graupel embryos in the two cases are similar, the accreted graupel content from the riming process in case A should not be greater than that in case B during short-term variation (the duration of graupel content variation does not exceed 6 minutes). However, the content is related to both the particle size and the number concentration. We retrieve the content from the echo intensity corresponding to the radar sample volume, and the determination of the nature of the radar sample volume depends mainly on the large particles (e.g., graupel). Thus, if there are more graupel particles distributed in more space, a greater sample volume of graupel in the radar corresponds to a greater graupel content.

The number concentration ($\log_{10}N_t$, L^{-1}) of ice particles (≤ 30 dBZ) when the first CI initiates at 18:00 (case A) or 12:06 (case B) is shown in Fig. 2e. Ice particles are potential sources of graupel embryos (Bringi et al., 1997; Carey and Rutledge, 2000). Moreover, the radar sample volume of the graupel particles clearly corresponds to a larger volume in case A (Fig. 2f). Thus, the observational characteristics support the above hypothesis; namely, the number concentration of graupel particles in case A is greater than that in case B, resulting in a clearly greater graupel content derived from radar in case A.

A greater number concentration of graupel depends on the increasing number concentration of graupel embryos. However, why are there more graupel embryos? Ice crystals and supercooled raindrops are the main sources of graupel embryos (Bringi et al., 1997; Carey and Rutledge, 2000). While the mechanism through which secondary ice production occurs increases the number concentration of ice crystals, we do not agree that these secondary ice crystals grow into graupel-sized particles within a few minutes. In light of the previous hypothesis and observations, we believe that the raindrops freeze into graupel particles should dominate the graupel formation during the initial phase of warm-based thunderstorms. The phase transition can be completed in a few minutes. Therefore, increasing the number concentration of supercooled raindrop-sized particles can increase the number concentration of graupel within 6 minutes.

b. How do supercooled raindrops increase in the first pre-CI?

Naturally, we seek to determine how the number of supercooled raindrops increases during the first pre-CI. The polarimetric "fingerprint" of warm-rain processes is quantified in Fig. 2g, h. Each colored dot indicates the changed Z_{DR} and Z_H values over an approximate 3-km rain shaft from one radar volume scan at different times. Warm-rain processes clearly differ between cases A and B. In case B (Fig. 2h), raindrops continuously undergo size sorting or evaporating processes; the stronger CAPE (1504 J kg^{-1}) and wind shear account for this difference (Williams et al., 2005; Carey and Buffalo, 2007; Fuchs et al., 2018; Stough et al., 2021). Not only does the ERA-Interim reanalysis data indicate greater wind shear in case B than in case A (Fig. 1b), but the positive Z_{DR} column from the cloud base to the mixed-phase layer in case B is also more tilted than that in case A (Fig. 1i, j).

In case A (Fig. 2g, i), the raindrops undergo size sorting or evaporation first, and then, the liquid drops are more likely to experience cyclic growth by coalescence under upright airflows and/or possibly weaker updrafts (smaller CAPE, 1277 J kg^{-1}) (Mather et al., 1986; Kumjian et al., 2014; Stough et al., 2021); thus, these raindrops coalesce at two subsequent moments, and large raindrops form (exceeding 2 mm). However, aerodynamic deformation causes these raindrops to break into many raindrops at 17:42 and/or 17:48, after which these raindrops can be easily lofted and/or participate in the coalescence process (i.e., 17:54 and 18:00). The breakup of raindrops at 17:42 and/or 17:48 accounts for the sharply increasing amount of supercooled rainwater, which is noted above in Fig. 2a, b.

Therefore, the weaker environmental wind shear and CAPE promote raindrop breakup in case A, and more raindrops are lofted to areas of subfreezing temperatures and freeze into graupel with higher number concentrations but fewer riming processes. We call this underlying mechanism "breakup–freezing", which is a hypothesis and is likely an important way to clarify the formation

https://doi.org/10.5194/egusphere-2026-4
Preprint. Discussion started: 2 February 2026

of thunderstorms with less significant CAPE and weak wind shear. In contrast, the stronger the environmental wind shear and CAPE are, the more likely it is that more droplets are lifted to areas of subfreezing temperatures and feed less graupel but moderately or heavily riming; this mechanism is similar to those of previous hypotheses (Carey and Buffalo, 2007; Fuchs et al., 2018; Stough et al., 2021). Naturally, we focus on the following question: after the first CI event (i.e., when convective clouds have developed into maturity and produced lightning or precipitation), does the "breakup–freezing" mechanism dominate the subsequent CI events, especially for thunderstorms that are near stationary (i.e., when surface sensible heating is suppressed by rainfall and radiation heating of the surface is weakened by thunderclouds)?

3.4. Why do subsequent CI events occur?

The logarithmic total water and ice contents and the lightning frequency in cases A and B during the second pre-CI event are displayed in Fig. 3a, b, c and d. In general, the contents of liquid water and ice decrease first with decreasing lightning frequency, indicating that the convection intensity is weakening and that rainfall is occurring. However, when the second CI initiates at 18:24 in case A, the supercooled raindrop content increases (Fig. 3a), whereas the graupel content does not increase at 18:24 (Fig. 3c); it obviously increases to $10^{7.3}$ kg at the next radar volume scan (18:30). Similarly, the supercooled raindrop content and graupel content increase when the second CI initiates at 12:48 in case B (Fig. 3b, d).

The frequency of the Z_H values (>35 dBZ) in every height layer (a vertical resolution of 500 m over 0.5 to 20 km of a radar volume scan) is shown in Fig. 3e and f, the height of the Z_H values (>35 dBZ) tends to decrease during the second pre-CI period, and the height is lower than the 0°C isotherm height. These characteristics indicate that the graupel particles fall into the warm-phase layer and melt, which can lead to the formation of large raindrops by melting and/or small raindrops by shedding in a short time (Wisner et al., 1972; Rasmussen and Heymsfield, 1987a, b, c). The melting and shedding behavior of graupel is significantly affected by its initial size (Rasmussen and Heymsfield, 1987b). Smaller graupel particles preferentially melt faster than large particles do (Rasmussen and Heymsfield, 1987b). The shedding of graupel can be an important source of new raindrops (Wisner et al., 1972); the rate of shedding depends on the graupel size, and larger graupel

https://doi.org/10.5194/egusphere-2026-4
Preprint. Discussion started: 2 February 2026

produces more shedding (Rasmussen and Heymsfield, 1987b). These findings indicate that the behaviors of melting and shedding with respect to graupel size are inversely related.

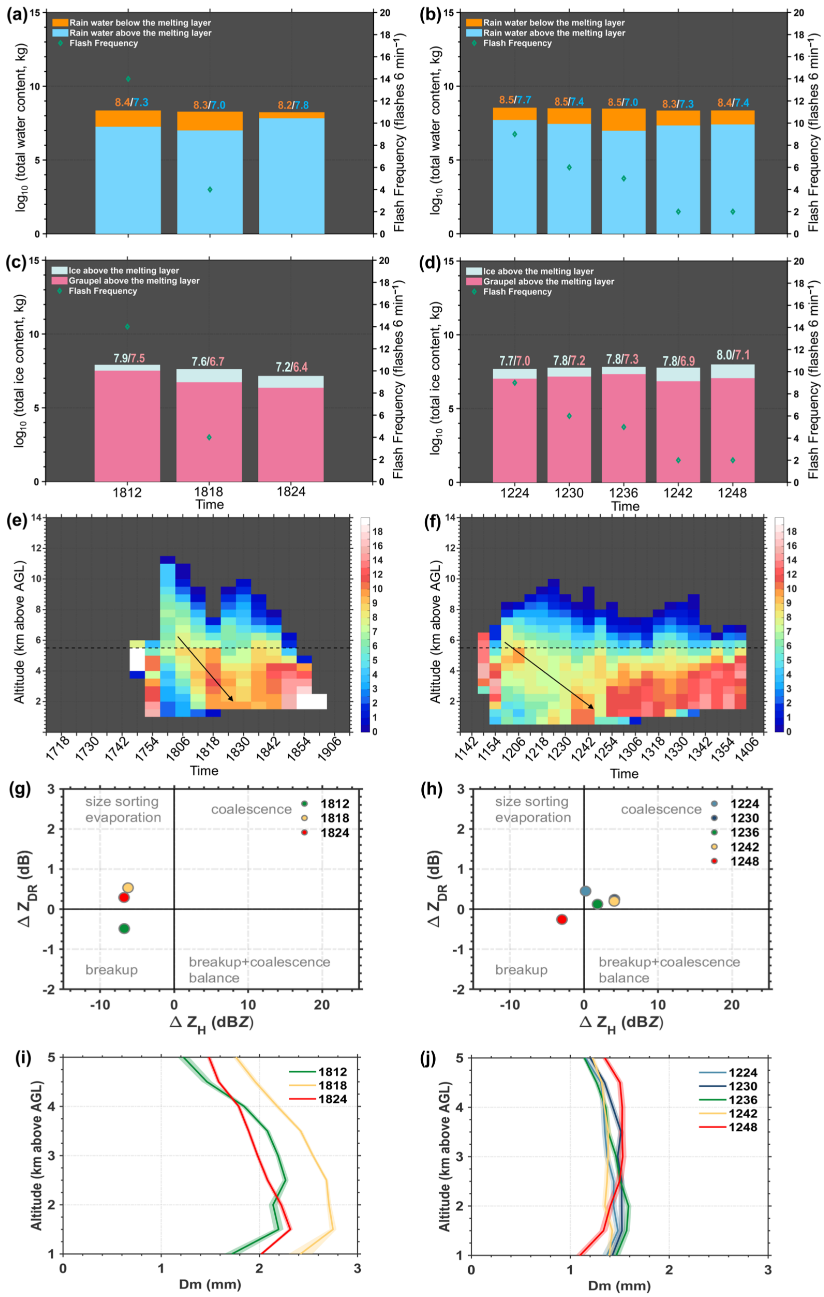

https://doi.org/10.5194/egusphere-2026-4
Preprint. Discussion started: 2 February 2026

Figure 3. Cloud microphysics during the second pre-CI period. The left column indicates that case A occurred on 20 June 2016. The right column indicates that case B occurred on 13 June 2016. (**a**) and (**b**) Histogram plots for the logarithmic total water content. The orange (blue) bars indicate the rainwater content below (above) the melting layer. (**c**) and (**d**) Histogram plots for the logarithmic total ice content. The cyan and pink bars indicate the contents of ice and graupel above the melting layer, respectively. The numerical values in different colors correspond to the total contents of different hydrometeors (unit, kg). The green diamond indicates the flash frequency. (**e**) and (**f**) The frequency in every height layer (a vertical resolution of 500 m over 0.5 to 20 km of a radar volume scan) of Z_H>35 dBZ, and the black arrows indicate the approximate direction of movement of high-frequency areas with cloud development during the second pre-CI period. The dashed black line indicates the 0°C isotherm height. The change in Z_{DR} vs. the change in Z_H over an approximately 3-km rain shaft and the microphysical processes represented by each quadrant or "fingerprint" are annotated: (**g**) case A and (**h**) case B. Each colored dot indicates the changed values of Z_{DR} and Z_H over an approximately 3-km rain shaft from one radar volume scan at different times. The retrieved mass-weighted mean drop diameter (D_m) is shown in (**i**) (case A) and (**j**) (case B), the lines indicate the mean values and the shaded area indicates the 95% confidence interval.

The data in Fig. 3g and h show that raindrop breakup occurred during the second pre-CI period; however, the occurrence time in case A differed from that in case B. Specifically, the occurrence time of raindrop breakup in case A was earlier than that in case B. The coalescence process was absent in case A, but raindrop breakup occurred, corresponding to graupel melting. This suggests that the large raindrops that break may have formed by the complete melting of smaller graupel in a shorter time. In addition, the coalescence process occurred before raindrop breakup in case B, and the small raindrops involved in the coalescence process may have resulted from shedding (Wisner et al., 1972; Rasmussen and Heymsfield, 1987a). This opinion is validated via retrieved raindrops D_m (Fig. 3i, j). In case B, the graupel size would be larger than that in case A (larger maximum Z_H values and a lower concentration of graupel in case B (Fig. 1 and Fig. 2e, f)). Thus, the larger graupel in case B preferentially produces small raindrops from shedding when the particles fall below the 0°C isotherm height; the rate of melting is lower than that in case A.

On the basis of the above characteristics and analysis, we suggest that the smaller graupel in case A easily melted into large raindrops (>2 mm, Fig. 3i) in a shorter time, after which the upright airflow promoted raindrop breakup. The precipitation loading, melting, evaporation and upright behavior of the storm affected the updraft intensity, resulting in a delay of broken raindrops from the warm phase lifting to areas of subfreezing temperatures. The larger graupel in case B preferentially produces small raindrops from shedding (<2 mm, Fig. 3j) in tilted downdrafts, and small raindrops may undergo coalescence to form large raindrops in tilted downdrafts (these large raindrops may reduce the evaporation rate (Pruppacher and Klett, 1997)), followed by breaking into

https://doi.org/10.5194/egusphere-2026-4
Preprint. Discussion started: 2 February 2026

many raindrops and reentering into low-level updrafts. Finally, the stronger updrafts at a low level in case B (likely resulting from moving and organizing air flow, and less consumption by evaporation) lifts raindrops to subfreezing temperatures in a shorter time than those in case A do.

Therefore, abundant raindrops produced by raindrop breakup and lifting to subfreezing temperatures account for the increased supercooled rainwater and graupel contents and the latent heat released to increase the convective intensity within clouds. Notably, while the "breakup–freezing" mechanism likely provided the kinematic source for the second CI, the methods of producing large raindrops to break differed between the second pre-CI period and the first pre-CI period. Moreover, the loading, melting and evaporation of precipitation likely reduced the net kinematic intensity for the second CI, resulting in the echo-top heights gradually decreasing during such CI events (Fig. 1c, d, e, f).

3.5. Physical basis for the "breakup–freezing" hypothesis in model simulations

To support our hypothesis, a sensitivity experiment is conducted with the Weather Research and Forecasting (WRF) model to investigate the effects of raindrop breakup (parameterization follows that of Verlinde and Cotton (1993)) on the number concentration of graupel and on the convective intensity (updraft velocity) within clouds. This is an ideal simulation. The physical options include only microphysical parameterization (Morrison two-moment) (Morrison et al., 2009).

In the first experiment, raindrop breakup is considered (hereafter RB); in the second experiment, no raindrop breakup parameterization is used (hereafter noRB). The WRF output information shows the difference between the RB and noRB experiments (Fig. 4); the evolution of the reflectivity and z-wind component in the RB experiment are shown in Figs. S4 and S5. The modeled convection starts at the 13th minute, and compared with the noRB experiment, the RB experiment clearly has a greater raindrop number concentration at the 15th, 16th, and 17th minutes (Fig. 4a, b, and c). Similarly, a higher graupel number concentration (Fig. 4e, f) and a stronger z-wind component (Fig. 4h, i) occurred during the 16th and 17th minutes of the RB experiment. Thus, the "breakup–freezing" mechanism has a physical basis for explaining the formation of CI events.

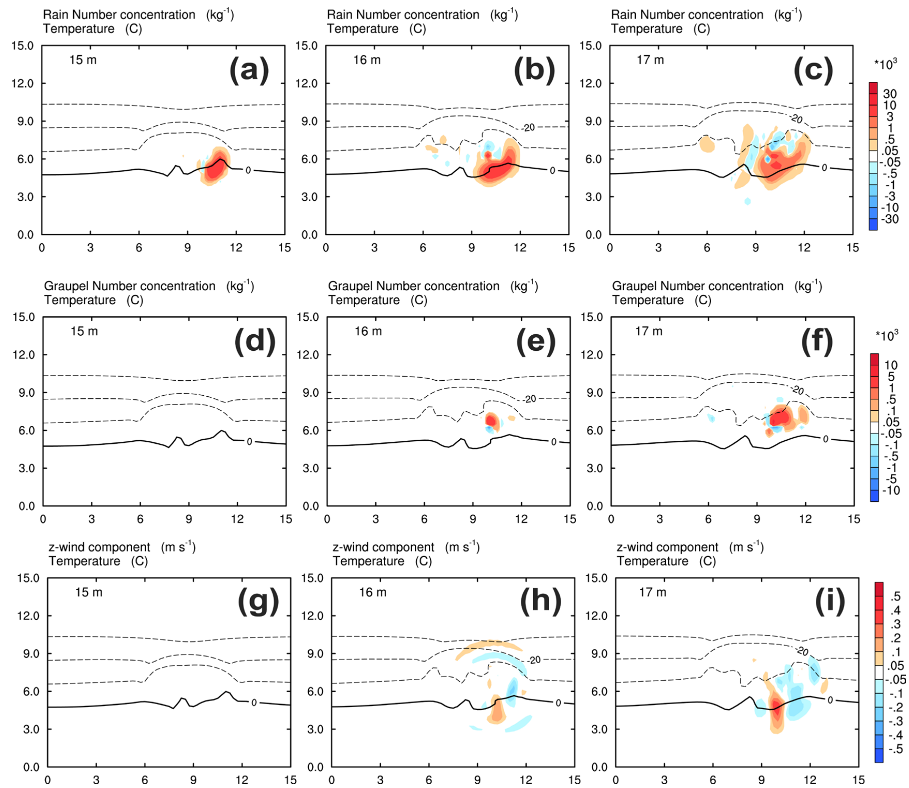

Figure 4. Output of the Weather Research and Forecasting (WRF) model. Two sensitivity experiments are conducted to investigate the effects of raindrop breakup on the number concentration of graupel and on the convective intensity (updraft velocity) within clouds. In the first experiment, raindrop breakup is considered (hereafter RB); in the second experiment, none of the raindrop breakup parameterizations are used (hereafter noRB). This figure shows the differences between the RB and noRB experiments. Rain number concentrations at (**a**) 15th minute, (**b**) 16th minute, and (**c**) 17th minute. Graupel number concentration at (**d**) the 15th minute, (**e**) 16th minute, and (**f**) 17th minute. (**g**), (**h**) and (**i**) indicate the z-wind components at the 15th minute, 16th minute and 17th minute, respectively. The black lines indicate the 0°C, −10°C, −20°C, and −30°C isotherm heights.

4. Conclusion and discussion

In this study, we collected multiple CI events within two isolated thunderstorms on the basis of observations from a polarimetric radar and lightning location system. The convective intensity indicated by the lightning frequency, echo-top height of 50 dBZ, and maximum Z_H value clearly displayed short-term impulses during the evolutionary cycles of two isolated thunderstorms (case A: 20 June 2016; case B: 13 June 2016) over southern China. Two CI events and two corresponding pre-CI events in each thunderstorm were defined.

https://doi.org/10.5194/egusphere-2026-4
Preprint. Discussion started: 2 February 2026

By comparing the microphysical characteristics between the thunderstorms in cases A and B from the first pre-CI event to the initial moment of the first CI event, we propose a hypothesis "breakup–freezing" mechanism to potentially explain the convective enhancement in the first CI event with a less significant CAPE, weak wind shear, and clean environment. For significant CAPE, strong wind shear and a clean environment, which followed the previous hypothesis for convective enhancement based on faster updrafts in the environment, resulted from the stronger CAPE, as described in Stough et al. (2021).

This "breakup–freezing" mechanism dominated the subsequent CI events in these two thunderstorms, although the methods for forming large raindrop breakup differed from those dominated by droplet cyclic growth coalescence in the first pre-CI. Large raindrops are formed by the complete melting of smaller graupel or by the coalescence of small raindrops from the shedding of larger graupel. This is important for understanding the enhancement of convection after precipitation loading, melting, and evaporation with a near-stationary thunderstorm cell.

Finally, a sensitivity experiment was conducted with the WRF model to investigate the effects of raindrop breakup on the number concentration of graupel and on the convective intensity within clouds. The simulation results confirmed that the "breakup–freezing" mechanism provided a physical basis for explaining the formation of CI events. The conceptual model in Fig. 5 illustrates the "breakup–freezing" mechanism for the enhancement of convection.

CAPE and wind shear are stronger in case B than in case A. Notably, the thunderstorm in case A is nearly stationary (indicating that surface sensible heating is suppressed by rainfall and that radiation heating of the surface is weakened by thunderclouds), but that in case B is moving frequently.

For the first CI event, two mechanisms account for the convective enhancement: 1) the less significant CAPE and weak wind shear promote large raindrop (>2 mm) formation by coalescence, and then, the large raindrops are transferred into many smaller raindrops by breakup in vertical air flow. These raindrops can be easily lifted to subfreezing temperatures and freeze into graupel with a higher number concentration. The latent heat released from raindrop freezing triggered the first CI event (Fig. 5a, b). 2) The significant CAPE and strong wind shear preferentially lift more cloud

https://doi.org/10.5194/egusphere-2026-4
Preprint. Discussion started: 2 February 2026

droplets to subfreezing temperatures and feed less graupel but with moderate or heavy riming, releasing latent heat to increase convection intensity (Fig. 5e, f).

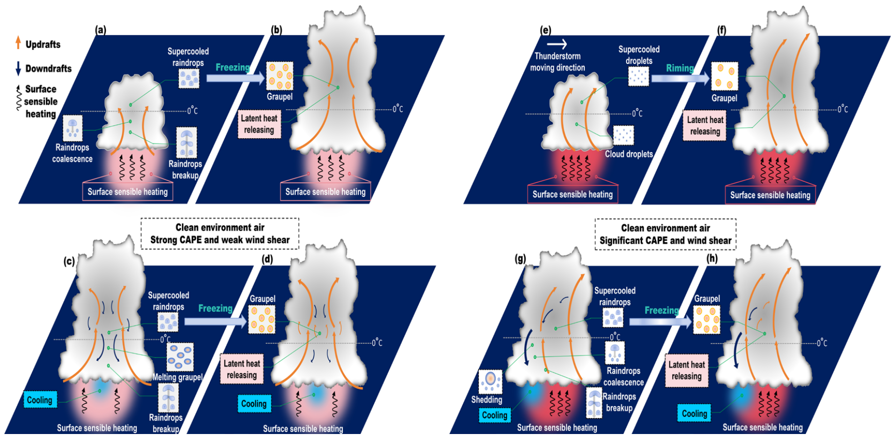

Figure 5. A conceptual model of the breakup–freezing mechanism for convective impulses. Convective impulses (CIs) are identified on the basis of radar and lightning observations in this study. CI events in the evolutionary cycle of isolated thunderstorm cells (case A: 20 June 2016; case B: 13 June 2016) over southern China are studied. The transitions from the first pre-CI stage to the first CI stage are shown in (**a**) and (**b**) (case A) and (**e**) and (**f**) (case B). In case A, the strong CAPE and weak wind shear promote the formation of large raindrops via coalescence, and many raindrops produced by large raindrop breakup are lifted to subfreezing temperatures and then freeze, and abundant graupel forms and releases latent heat. However, in case B, the significant CAPE and strong wind shear suppress the warm rain processes. More cloud droplets are lifted to subfreezing temperatures, promoting the riming process, the formation of graupel and the release of latent heat. The transitions from the second pre-CI stage to the second CI stage are shown in (**c**) and (**d**) (case A) and in (**g**) and (**h**) (case B). The smaller graupel in case A easily melts into large raindrops, after which the raindrops break up in the vertical air flow. The many raindrops produced by large-sized raindrop breakup are lifted to subfreezing temperatures and then freeze, leading to the formation of abundant graupel and the release of latent heat. In case B, the larger graupel particles preferentially become small raindrops from shedding in tilted downdrafts, and large raindrops form through small raindrop coalescence in tilted downdrafts, followed by breaking to many raindrops and reentering into updrafts. Finally, the stronger updrafts lift these smaller raindrops into areas of subfreezing temperatures, where they turn into graupel and release latent heat.

During the second pre-CI period, negative buoyancy is produced by latent heat cooling and precipitation loading. The surface sensible heating is suppressed, and the energy for triggering the second CI event is unlikely to be sourced from increasing surface energy, especially for that in the near-stationary case A. However, the smaller graupel in case A easily melts into large raindrops and then breaks up in the vertical air flow. These raindrops produced by large raindrop breakup are lifted to subfreezing temperatures and then freeze, leading to the formation of abundant graupel and the release of latent heat, thus triggering the second CI event (Fig. 5c, d).

https://doi.org/10.5194/egusphere-2026-4
Preprint. Discussion started: 2 February 2026

However, the larger maximum Z_H values and lower concentration of graupel indicate greater graupel in case B. These large graupel particles preferentially produce small raindrops from shedding in tilted downdrafts instead of rapid melting into large raindrops (Wisner et al., 1972; Rasmussen and Heymsfield, 1987a, b, c). Small raindrops are transformed into large raindrops by coalescence in tilted downdrafts. Large raindrops subsequently break into many raindrops and reenter low-level updrafts. Finally, the updrafts lift these smaller raindrops into areas of subfreezing temperatures, where they turn into graupel and release latent heat (Fig. 5g, h). Notably, the period between large raindrop breakup and the second CI event initiated in case B is shorter than that in case A, which is due to the stronger updrafts at a low level in case B (the construction of tilted air flows and moving behavior and less consumption by evaporation may be beneficial to the updrafts). Notably, the net kinematic intensity for the second CI is weaker than that for the first CI via latent heat cooling and precipitation loading.

Although this study provides the hypothesis "breakup–freezing" mechanism for trying to explain the formation of CI events, there is estimated error in the inferred cloud microphysics. Fortunately, our results are drawn from the analysis of the comparison, which minimizes the effects of estimated errors. However, how to quantitatively estimate microphysics more accurately is the key to parameterizing the "breakup–freezing" mechanism into weather or climate numerical simulation models. This will improve the results of simulations of severe storms.

Acknowledgments

The authors acknowledge the Guangzhou Institute of Tropical and Marine Meteorology for collecting and archiving the radar and surface observations. And authors also acknowledge the State Key Laboratory of Severe Weather Meteorological Science and Technology & CMA Key Laboratory of Lightning for three-dimensional lightning location data.

Financial support

This research has been supported by the National Natural Science Foundation of China (grant nos. 42175090, 42305079 and 42075088), the Open Research Fund Project of the Joint Laboratory for Phased-Array Weather Radar Applications in the East China Region (grant no. EPJL_JF2025001), and the China Postdoctoral Science Foundation (grant no. 2023M730619).

https://doi.org/10.5194/egusphere-2026-4
Preprint. Discussion started: 2 February 2026

Author contributions:

Conceptualization: CZ and YZ. Data curation: CZ, YZ, DZ and WY. Formal analysis: CZ, YZ and LX. Funding acquisition: YZ, CZ and LX. Investigation: CZ, YZ and LX. Methodology: CZ, YZ, DZ and LX. Project administration: YZ. Resources: CZ and YZ. Software: CZ and DZ. Supervision: YZ and CZ. Validation: CZ and YZ. Visualization: CZ and YZ. Writing (original draft): CZ, YZ and LX.

Competing interests:

The contact author has declared that none of the authors has any competing interests.

Data and materials availability: All data in this study can be obtained from an open repository Figshare (Zhao, 2024).

References

Beard, K. V.: Ice initiation in warm-base convective clouds: An assessment of microphysical mechanisms. Atmospheric Research, 28(2): 125–152, https://doi.org/10.1016/0169-8095(92)90024-5, 1992.

Braham, R. R. Jr.: The cloud physics of weather modification. Part 1: Scientific basis. WMO Bulletin, 35, 215–221, 1986.

Bringi, V. N., Knupp, K., Detwiler, A., Liu, L., Caylor, I. J. and Black, R. A.: Evolution of a Florida Thunderstorm during the Convection and Precipitation/Electrification Experiment: The Case of 9 August 1991. Monthly Weather Review, 125(9): 2131–2160, https://doi.org/10.1175/1520-0493(1997)125<2131:EOAFTD>2.0.CO;2, 1997.

Bringi, V. N. and Chandrasekar, V.: Polarimetric Doppler Weather Radar: Principles and Applications. Cambridge University Press, Cambridge, ISBN 978-0-521-62384-1, 2001.

Bruning, E. C., Brunner, K. N., van Lier-Walqui, M., Logan, T. and Matsui, T.: Lightning and Radar Measures of Mixed-Phase Updraft Variability in Tracked Storms during the TRACER Field Campaign in Houston, Texas. Monthly Weather Review, 152, 2753–2769, https://doi.org/10.1175/MWR-D-24-0060.1, 2024.

Carey, L. D. and Buffalo, K. M.: Environmental Control of Cloud-to-Ground Lightning Polarity in Severe Storms. Monthly Weather Review, 135, 1327–1353, https://doi.org/10.1175/MWR3361.1, 2007.

Carey, L. D. and Rutledge, S. A.: The Relationship between Precipitation and Lightning in Tropical Island Convection: A C-Band Polarimetric Radar Study. Monthly Weather Review, 128(8): 2687–2710, 10.1175/1520-0493(2000)128<2687:TRBPAL>2.0.CO;2, 2000.

Cecil, D. J., Buechler, D. and Blakeslee, R. J.: Gridded lightning climatology from TRMM-LIS and OTD: dataset description. Atmospheric Research, 135–136: 404–414,

https://doi.org/10.5194/egusphere-2026-4
Preprint. Discussion started: 2 February 2026

https://doi.org/10.1016/j.atmosres.2012.06.028, 2014.

Chen, L., Zhang, Y. J., Lyu, W., Zheng, D., Zhang, Y., Chen, S. and Huang, Z.: Performance evaluation for a lightning location system based on observations of artificially triggered lightning and natural lightning flashes. Journal of Atmospheric and Oceanic Technology, 29: 1835–1844, https://doi.org/10.1175/JTECH-D-12-00028.1, 2012.

Dagan, G., Stier, P., Christensen, M., Cioni, G., Klocke, D. and Seifert, A.: Atmospheric energy budget response to idealized aerosol perturbation in tropical cloud systems. Atmospheric Chemistry and Physics, 20: 4523–4544, https://doi.org/10.5194/acp-20-4523-2020, 2020.

Dee, D. P., Uppala, S. M., Simmons, A. J., Berrisford, P., Poli, P., Kobayashi, S., Andrae, U., Balmaseda, M. A., Balsamo, G., Bauer, P., Bechtold, P., Beljaars, A. C. M., van de Berg, L., Bidlot, J., Bormann, N., Delsol, C., Dragani, R., Fuentes, M., Geer, A. J., Haimberger, L., Healy, S. B., Hersbach, H., Hólm, E. V., Isaksen, L., Kållberg, P., Köhler, M., Matricardi, M., McNally, A. P., Monge-Sanz, B. M., Morcrette, J. J., Park, B. K., Peubey, C., de Rosnay, P., Tavolato, C., Thépaut, J. N. and Vitart, F.: The ERA-Interim reanalysis: configuration and performance of the data assimilation system. Quarterly Journal of the Royal Meteorological Society, 137: 553–597, https://doi.org/10.1002/qj.828, 2011.

Fan, J. W., Rosenfeld, D., Zhang, Y., Giangrande, S. E., Li, Z., Machado, L. A. T., Martin, S. T., Yang, Y., Wang, J., Artaxo, P., Barbosa, H. M. J., Braga, R. C., Comstock, J. M., Feng, Z., Gao, W., Gomes, H. B., Mei, F., Pöhlker, C., Pöhlker, M. L., Pöschl, U. and de Souza, R. A. F.: Substantial convection and precipitation enhancements by ultrafine aerosol particles. Science, 359: 411–418, 10.1126/science.aan8461, 2018.

Fan, J. W., Zhang,Y., Li, Z., Yan, H., Prabhakaran, T., Rosenfeld, D. and Khain, A.: Unveiling aerosol impacts on deep convective clouds: Scientific concept, modeling, observational analysis, and future direction. Journal of Geophysical Research: Atmospheres, 130: e2024JD041931, https://doi.org/10.1029/2024JD041931, 2025.

Fan, X. P., Zhang, Y. J., Zheng, D., Zhang, Y., Lyu, W. T., Liu, H. Y. and Xu, L. T.: A New Method of Three-Dimensional Location for Low-Frequency Electric Field Detection Array. Journal of Geophysical Research: Atmospheres, 123(16): 8792-8812, 10.1029/2017jd028249, 2018.

Fuchs, B. R., Rutledge, S. A., Dolan, B., Carey, L. D. and Schultz, C.: Microphysical and kinematic processes associated with anomalous charge structures in isolated convection. Journal of Geophysical Research: Atmospheres, 123: 6505–6528, https://doi.org/10.1029/2017JD027540, 2018.

Grabowski, W. W.: Daytime convective development over land: The role of surface forcing. Quarterly Journal of the Royal Meteorological Society, 149: 2800–2819, https://doi.org/10.1002/qj.4532, 2023.

Grabowski, W. W. and Morrison, H.: Do Ultrafine Cloud Condensation Nuclei Invigorate Deep Convection? Journal of the Atmospheric Sciences, 77: 2567–2583, https://doi.org/10.1175/JAS-D-20-0012.1, 2020.

Grabowski, W. W. and Morrison, H.: Supersaturation, buoyancy, and deep convection dynamics. Atmospheric Chemistry and Physics, 21: 13997–14018, https://doi.org/10.5194/acp-21-13997-2021, 2021.

Golestani, Y., Chandrasekar, V. and Bringi, V. N.: paper presented at the 24th Conference on Radar Meteorology, Tallahassee, FL, American Meteorological Society, 1989.

Herzegh, P. H. and Jameson, A. R.: Observing Precipitation through Dual-Polarization Radar

https://doi.org/10.5194/egusphere-2026-4
Preprint. Discussion started: 2 February 2026

Measurements. Bulletin American Meteorological Society, 73(9): 1365-1376, 10.1175/1520-0477(1992)073<1365:OPTDPR>2.0.CO;2, 1992.

Hu, J. and Ryzhkov, A.: Climatology of the Vertical Profiles of Polarimetric Radar Variables and Retrieved Microphysical Parameters in Continental/Tropical MCSs and Landfalling Hurricanes. Journal of Geophysical Research: Atmospheres, 127(5), 10.1029/2021jd035498, 2022.

Koren, I., Kaufman, Y. J., Remer, L. A. and Martins, J. V.: Measurement of the effect of Amazon smoke on inhibition of cloud formation. Science, 303: 1342–1345, 10.1126/science.1089424, 2004.

Kumjian, M. R., Khain, A. P., Benmoshe, N., Ilotoviz, E., Ryzhkov, A. V. and Phillips, V. T. J.: The Anatomy and Physics of ZDR Columns: Investigating a Polarimetric Radar Signature with a Spectral Bin Microphysical Model. Journal of Applied Meteorology and Climatology, 53(7): 1820-1843, 10.1175/jamc-d-13-0354.1, 2014.

Kumjian, M. R., Prat, O. P., Reimel, K. J., van Lier-Walqui, M. and Morrison, H. C.: Dual-Polarization Radar Fingerprints of Precipitation Physics: A Review. Remote Sensing, 14, 3706, https://doi.org/10.3390/rs14153706, 2022.

Kumjian, M. R. and Prat, O. P.: The Impact of Raindrop Collisional Processes on the Polarimetric Radar Variables. Journal of the Atmospheric Sciences, 71: 3052–3067, https://doi.org/10.1175/JAS-D-13-0357.1, 2014.

Li, H. Q., Wan, Q., Peng, D., Liu, X. and Xiao, H.: Multiscale analysis of a record-breaking heavy rainfall event in Guangdong, China. Atmospheric Research, 232: 104703. https://doi.org/10.1016/j.atmosres.2019.104703, 2019.

Liu, N., Liu, C., Chen, B. and Zipser, E.: What Are the Favorable Large-Scale Environments for the Highest-Flash-Rate Thunderstorms on Earth? Journal of the Atmospheric Sciences, 77: 1583–1612, https://doi.org/10.1175/JAS-D-19-0235.1, 2020.

Liu, Z., Zheng, D., Guo, F., Zhang, Y., Zhang, Y., Wu, C., Chen, H. and Han, S.: Lightning activity and its associations with cloud structures in a rainstorm dominated by warm precipitation. Atmospheric Research, 246, 10.1016/j.atmosres.2020.105120, 2020.

Lucas, C., Zipser, E. J. and Lemone, M. A.: Vertical Velocity in Oceanic Convection off Tropical Australia. Journal of the Atmospheric Sciences, 51: 3183–3193, https://doi.org/10.1175/1520-0469(1994)051<3183:VVIOCO>2.0.CO;2, 1994.

MacGorman, D. R. and Rust, W. D.: The Electrical Nature of Storms. Oxford University Press, ISBN 10: 0195073371, 1998.

Markowski, P. and Richardson, Y.: Mesoscale Meteorology in Midlatitudes. John Wiley and Sons Press, ISBN 9780470742136, 2010.

Mather, G. K., Morrison, B. J. and Morgan, G. M. Jr.: A Preliminary Assessment of the Importance of Coalescence in Convective Clouds of the Eastern Transvaal. Journal of Applied Meteorology and Climatology, 25: 1780–1784, https://doi.org/10.1175/1520-0450(1986)025<1780:APAOTI>2.0.CO;2, 1986.

Mattos, E. V., Machado, L. A. T., Williams, E. R., Goodman, S. J., Blakeslee, R. J. and Bailey, J. C.: Electrification life cycle of incipient thunderstorms. Journal of Geophysical Research: Atmospheres, 122: 4670–4697, https://doi.org/10.1002/2016JD025772, 2017.

Morrison, H., Thompson, G. and Tatarskii, V.: Impact of cloud microphysics on the development of trailing stratiform precipitation in a simulated squall line: Comparison of one- and two-moment

https://doi.org/10.5194/egusphere-2026-4
Preprint. Discussion started: 2 February 2026

schemes. Monthly Weather Review, 137: 991–1007, https://doi.org/10.1175/2008MWR2556.1, 2009.

Orville, R. E. and Henderson, R. W.: Global Distribution of Midnight Lightning: September 1977 to August 1978. Monthly Weather Review, 114: 2640–2653, https://doi.org/10.1175/1520-0493(1986)114<2640:GDOMLS>2.0.CO;2, 1986.

Pruppacher, H. R. and Klett, J. D.: Microphysics of Clouds and Precipitation. Kluwer Academic, ed. 2, ISBN 079234409X, 1997.

Qie, X., Yair, Y., Di, S., Huang, Z. and Jiang, R.: Lightning response to temperature and aerosols. Environmental Research Letters, 19: 083003, 10.1088/1748-9326/ad63bf, 2024.

Rasmussen, R. M. and Heymsfield, A. J.: Melting and Shedding of Graupel and Hail. Part I: Model Physics. Journal of the Atmospheric Sciences, 44: 2754–2763, https://doi.org/10.1175/1520-0469(1987)044<2754:MASOGA>2.0.CO;2, 1987a.

Rasmussen, R. M. and Heymsfield, A. J.: Melting and Shedding of Graupel and Hail. Part II: Sensitivity Study. Journal of the Atmospheric Sciences, 44: 2764–2782, https://doi.org/10.1175/1520-0469(1987)044<2764:MASOGA>2.0.CO;2, 1987b.

Rasmussen, R. M. and Heymsfield, A. J.: Melting and Shedding of Graupel and Hail. Part III: Investigation of the Role of Shed Drops as Hail Embryos in the 1 August CCOPE Severe Storm. Journal of the Atmospheric Sciences, 44: 2783–2803, https://doi.org/10.1175/1520-0469(1987)044<2783:MASOGA>2.0.CO;2, 1987c.

Rosenfeld, D. and Lensky, I. M.: Satellite-Based Insights into Precipitation Formation Processes in Continental and Maritime Convective Clouds. Bulletin of the American Meteorological Society, 79: 2457–2476, https://doi.org/10.1175/1520-0477(1998)079<2457:SBIIPF>2.0.CO;2, 1998.

Rosenfeld, D., Lohmann, U., Raga, G. B., O'Dowd, C. D., Kulmala, M., Fuzzi, S., Reissell, A. and Andreae, M. O.: Flood or Drought: How Do Aerosols Affect Precipitation? Science, 321(5894): 1309-1313, doi:10.1126/science.1160606, 2008.

Shi, D., Zheng, D., Zhang, Y., Zhang, Y., Huang, Z., Lu, W., Chen, S. and Yan, X.: Low-frequency E-field Detection Array (LFEDA)—Construction and preliminary results. Science China Earth Sciences, 60(10): 1896-1908, 10.1007/s11430-016-9093-9, 2017.

Smith, P. L., Musil, D. J., Detwiler, A. G. and Ramachandran, R.: Observations of Mixed-Phase Precipitation within a CaPE Thunderstorm. Journal of Applied Meteorology and Climatology, 38: 145–155, https://doi.org/10.1175/1520-0450(1999)038<0145:OOMPPW>2.0.CO;2, 1999.

Stolzenburg, M., Marshall, T. C. and Krehbiel, P. R.: Initial electrification to the first lightning flash in New Mexico thunderstorms. Journal of Geophysical Research: Atmospheres, 120: 11253–11276, https://doi.org/10.1002/2015JD023988, 2015.

Stough, S. M., Carey, L. D., Schultz, C. J. and Cecil, D. J.: Examining conditions supporting the development of anomalous charge structures in supercell thunderstorms in the Southeastern United States. Journal of Geophysical Research: Atmospheres, 126: e2021JD034582, https://doi.org/10.1029/2021JD034582, 2021.

Thornton, J. A., Virts, K. S., Holzworth, R. H. and Mitchell, T. P.: Lightning enhancement over major oceanic shipping lanes. Geophysical Research Letters, 44: 9102–9111, https://doi.org/10.1002/2017GL074982, 2017.

Tokay, A., D'Adderio, L. P., Marks, D. A., Pippitt, J. L., Wolff, D. B. and Petersen, W. A.: Comparison of Raindrop Size Distribution between NASA's S-Band Polarimetric Radar and

https://doi.org/10.5194/egusphere-2026-4
Preprint. Discussion started: 2 February 2026

Two-Dimensional Video Disdrometers. Journal of Applied Meteorology and Climatology, 59: 517–533, https://doi.org/10.1175/JAMC-D-18-0339.1, 2020.

Varble, A. C., Igel, A. L., Morrison, H., Grabowski, W. W. and Lebo, Z. J.: Opinion: A critical evaluation of the evidence for aerosol invigoration of deep convection. Atmospheric Chemistry and Physics, 23: 13791–13808, https://doi.org/10.5194/acp-23-13791-2023, 2023.

Verlinde, J. and Cotton, W. R.: Fitting Microphysical Observations of Nonsteady Convective Clouds to a Numerical Model: An Application of the Adjoint Technique of Data Assimilation to a Kinematic Model. Monthly Weather Review, 121: 2776–2793, https://doi.org/10.1175/1520-0493(1993)121<2776:FMOONC>2.0.CO;2, 1993.

Wang, X. and Zhang, R.: Effects of atmospheric circulations on the interannual variation in PM2.5 concentrations over the Beijing–Tianjin–Hebei region in 2013–2018. Atmospheric Chemistry and Physics, 20: 7667–7682, https://doi.org/10.5194/acp-20-7667-2020, 2020.

Williams, E. R. and Stanfill, S.: The physical origin of the land-ocean contrast in lightning activity. Comptes Rendus Physique, 3: 1277–1292, https://doi.org/10.1016/S1631-0705(02)01407-X, 2002.

Williams, E. R., Mushtak, V., Rosenfeld, D., Goodman, S. and Boccippio, D.: Thermodynamic conditions favorable to superlative thunderstorm updraft, mixed phase microphysics and lightning flash rate. Atmospheric Research, 76: 288–306, https://doi.org/10.1016/j.atmosres.2004.11.009, 2005.

Wisner, C., Orville, H. D. and Myers, C.: A Numerical Model of a Hail-Bearing Cloud. Journal of the Atmospheric Sciences, 29: 1160–1181, https://doi.org/10.1175/1520-0469(1972)029<1160:ANMOAH>2.0.CO;2, 1972.

Zhang, Y., Yan, M., Sun, A. and Guo, F.: Thunderstorm Electricity, China Meteorology Press, Beijing, 384 pp., ISBN 9787502947682, 2009.

Zhao, C.: Data for “Physical Interpretation and Implications of Convective Impulses in Thunderstorms Based on Lightning and Polarimetric Radar Observations”. figshare. [Dataset]. https://doi.org/10.6084/m9.figshare.26779426.v4, 2024.

Zhao, C., Zhang, Y., Zhai, H., Li, Z., Zheng, D., Peng, X., Yao, W., Du, S. and Du, Y.: Bridging the polarimetric structure and lightning activity of isolated thunderstorm cells during the cloud life cycle. Atmospheric Chemistry and Physics, 25: 13453–13473, https://doi.org/10.5194/acp-25-13453-2025, 2025.

Zhao, C., Zhang, Y., Zheng, D., Li, H., Du, S., Peng, X., Liu, X., Zhao, P., Zheng, J. and Shi, J.: Technical note: On the ice microphysics of isolated thunderstorms and non-thunderstorms in southern China – a radar polarimetric perspective. Atmospheric Chemistry and Physics, 24(20): 11637-11651, 10.5194/acp-24-11637-2024, 2024a.

Zhao, C., Zhang, Y., Zheng, D., Liu, X., Zhang, Y., Fan, X., Yao, W. and Zhang, W.: Using Polarimetric Radar Observations to Characterize First Echoes of Thunderstorms and Nonthunderstorms: A Comparative Study. Journal of Geophysical Research: Atmospheres, 127(23): e2022JD036671, https://doi.org/10.1029/2022JD036671, 2022.

Zhao, C., Zhang, Y. J., Zheng, D., Yao, W. and Du, S.: Potential Method for Warning the First Lightning Flash of Isolated Thunderstorm Cells over South China. Weather and Forecasting 40: 105–115, https://doi.org/10.1175/WAF-D-23-0189.1, 2024b.

Zhao, C., Zheng, D., Zhang, Y. J., Liu, X., Zhang, Y., Yao, W. and Zhang, W.: Characteristics of cloud microphysics at positions with flash initiations and channels in convection and stratiform

https://doi.org/10.5194/egusphere-2026-4
Preprint. Discussion started: 2 February 2026

areas of two squall lines, Journal of Tropical Meteorology, 37: 358–369, doi:10.16032/j.issn.1004-4965.2021.035, 2021a.

Zhao, C., Zheng, D., Zhang, Y. J., Liu, X., Zhang, Y., Yao, W. and Zhang, W.: Turbulence Characteristics of Thunderstorms Before the First Flash in Comparison to Non-Thunderstorms. Geophysical Research Letters, 48(18): e2021GL094821, https://doi.org/10.1029/2021GL094821, 2021b.

Zheng, D., Shi, D., Zhang, Y., Zhang, Y. J., Lyu, W. and Meng, Q.: Initial leader properties during the preliminary breakdown processes of lightning flashes and their associations with initiation positions. Journal of Geophysical Research: Atmospheres, 124: 8025–8042, https://doi.org/10.1029/2019JD030300, 2019.

Zipser, E. J., Cecil, D. J., Liu, C., Nesbitt, S. W. and Yorty, D. P.: WHERE ARE THE MOST INTENSE THUNDERSTORMS ON EARTH? Bulletin of the American Meteorological Society, 87: 1057–1072, https://doi.org/10.1175/BAMS-87-8-1057, 2006.